Egypt. J. Chem. **Vol. 65,** No. 3 pp. 51 - 72 (2022)

Egyptian Journal of Chemistry

http://ejchem.journals.ekb.eg/

Synthesis, Characterization, Electrochemical Studies and Biological Activities of Complexes of Tridentate Schiff Base Ligand with Divalent Metal Ions

A.Z. El-Sonbati[a,*], M.A. Diab[a], R.A. El-Fayoumy[b], A.M. Eldesoky[c], S.A. El-Sayad[a]

[a] *Chemistry Department, Faculty of Science, Damietta University, Damietta, Egypt*

[b] *Botany and Microbiology Department, Faculty of Science, Damietta University, Damietta, Egypt*

[c] *Engineering Chemistry Department, High Institute of Engineering &Technology (New Damietta), Egypt and Al-Qunfudah Center for Scientific Research (QCSR), Chemistry Department, Al-Qunfudah University College, Umm Al-Qura University, KSA*

Abstract

A series of novel Schiff base 1-((2-hydroxyphenyl)iminomethyl)naphthalene-2-ol (H_2L) and its Cu(II), Co(II), Ni(II), Mn(II),Cd(II) and UO_2(II) complexes were synthesized and characterized. The nature of bonding and the geometry of the complexes were deduced from elemental analysis, spectral (FT-IR, UV-Vis., ^{1}H NMR, mass and ESR), magnetic moment, thermal analyses, X-ray diffraction and conductivity measurements. The microbial activity of the compounds was studied using disc diffusion method against bacteria, *Staphylococcus aureus*, *Escherichia coli*, *Pseudomonas aeruginosa*, *Klebsiella pneumonia* and *Bacillus subtilis* and against fungi, *Aspergillus niger*, *Fusarium oxysporum*, *Alternaria alternata* and *Candida albicans.* The results indicated that the Ni(II) complex showed the potent antibacterial activities against *Staphylococcus aureus* and *Klebsiella pneumoniae* only at 150 µg/mL. The data showed that the antifungal effect of ligand against *A. niger* was similar to the effect of Co(II), Mn(II), Cd(II) and UO_2(II) complexes where the inhibition zone ranged from 23-26 mm at 150 µg/mL concentration .The ligand showed higher interaction value of receptor of *Staphylococcus aureus* (3q8u) than receptor of *Escherichia coli* (3t88).The inhibition process of the prepared ligand (H_2L) against the corrosion of Concrete Steel Reinforcement in HCl (2 M) solution was determined by various electrochemical methods are found to be in reasonable agreement.

***Keywords*:** Schiff base ligand; Metal complexes; Characterization; Molecular docking; Biological activities; Steel-reinforced concrete.

1. Introduction

Schiff base complexes have a variety of applications in biology and analytical fields [1-5].The chemistry of Schiff base complexes is fast developing, especially those involving aldehydes and amines. This is because of the wide variety of possible structure of ligands [6-8].

Schiff base ligands and their metal complexes derived from 4-aminoantipyrine are essential due to their important applications in industrial field, catalytically, biological, biochemical, analytical field, and medicinally useful metal chelates [1-5,9]. Schiff bases represented an important class of organic compounds, especially in the medicinal and pharmaceutical fields. Thus, development and synthesis of new Schiff base derivatives still attract the attention of organic and medicinal chemists as their use as potential chemotherapeutics [10].

This article reports the syntheses and characterization of a series of novel Schiff base1-((2-hydroxyphenyl)iminomethyl)naphthalene-2-ol (H_2L) and its Cu(II), Co(II), Ni(II), Mn(II),Cd(II) and UO_2(II) complexes using different techniques. The structure of the complexes is proposed**.** The synthesized compounds were studied for their microbial activity using disc diffusion method against some bacteria, namely *Staphylococcus aureus, Escherichia coli, Pseudomonas aeruginosa, Klebsiella pneumoniae* and *Bacillus subtilis* as well as against some fungi such as *Aspergillus niger, Fusarium oxysporum, Alternaria alternata* and *Candida albicans*.

*Corresponding author e-mail: elsonbatisch@yahoo.com.; (A.Z. El-Sonbati).

EJCHEM use only: Receive Date: 13 June 2021, Revise Date: 28 August 2021, Accept Date: 12 September 2021

DOI: 10.21608/ejchem.2021.80432.3989

2. Experimental

2.1. Materials and Instrumentations.

All the chemicals used were AR quality. 2-hydroxy-1-naphthaldehyde and 2-aminophenol, sodium chloride and dimethylformamide (DMF) were procured from Sigma Aldrich. All the solvents were purified by distillation and used. All measurements were carried out as reported earlier [11-17].

The Schiff base was prepared by refluxing 2-hydroxy-1-naphthaldehyde with 2-aminophenol (1:1, in ethanol) for two hour, when the ligand (H_2L) was obtained as yellow color solid (Fig. S1). The purity was checked by TLC and m.p. is 186 ±2 ^oC.

The metal chelates of H_2L were synthesized by refluxing ethanolic solutions of respective metal acetates (0.01 mol) and the H_2L (0.01 mol) for ~ 2-3 hrs and keeping the reaction mixtures overnight. The respective metal chelates that separated out were filtered, washed successively with hot solvent followed by ether and dried in vacuum (Fig. 1).

2.2. Biological analysis

2.2.1 Tested Bacterial and Fungal strains

The antimicrobial test was performed against two Gram positive pathogenic bacteria (*Bacillus subtilis* and *Staphylococcus aureus*), three Gram negative pathogenic bacteria (*Escherichia coli, Pseudomonas aeruginosa*, and *Klebsiella pneumoniae*) and four fungal strains (*Aspergillus niger, Fusarium oxysporum, Candida albicans* and *Alternaria alternata*) [18-22].The media used for the microbial growth were nutrient broth, Dox agar and Nutrient agar.

2.2.2 Bacterial and fungal cultures preparation

Cultures of the five tested bacterial strains were prepared and characterized according to the previously reported method [18-22]**.**

2.2.3 Preparation of the compounds

50, 100 and 150 µg/mL concentrations of the synthesized compounds were prepared by using dimethylformamide (DMF) as solvent and then screened for detection of antibacterial and antifungal activities

2.2.4 The Antimicrobial assay

The antibacterial and antifungal activity of the synthesized compounds against the tested pathogenic microbes was evaluated as in traditional antibiotic susceptibility testing using the disc diffusion method **[**23-26**]**.

2.2.5 Statistical analysis

The statistical analyses were carried out using SPSS (version 22). The obtained data of degree of significance were analyzed statistically using a one way and three-way analysis of variance (ANOVA) at probability level $p \leq 0.05$. Results are presented as the mean ± standard error (SE) of two replicates.

2.3. Corrosion measurements

2.3.1. Metal coupons composition and medium

Steel-reinforced concrete was utilized for the calculation of corrosion. Its percent composition is 98% Fe, 0.273% C, 0.780% Mn, 0.403% Si and trace percentages of Cu, Cr, Ni P S, Mo Co Nb, Sn, Ce and V. The corrosion concentration (2 M HCl) (37% analytical grade,) was ready by hydrochloric acid dilution with double distilled water.

2.3.2. Potentiodynamic polarization measurements (TP)

TP test were performed using a Gamry Galvanostat/ZRA/ Potentiostat (model PCI 300/4) by three electrodes include the reference electrode (SCE) and platinum sheetas a counter electrode. The steel-reinforced concrete electrode coins was cut square from steel-reinforced concrete of size (1×1 cm) and was fused by one side to a copper wire, TP testes were carried out at 25 ± 0.1 °C from -5 to 5 V and scan rate 0.5 mVs^{-1}.

2.3.3. Electrochemical Frequency Modulation technique (EFM)

EFM can be utilizing for determine the rate of corrosion in non-attendance of prior data of Tafel constants. It was achieved by employed (2.0 to 5.0 Hz).The Intermodulation spectra contain current gotten from corrosion ($i_{corr.}$). The greater peaks were utilized to calculate the EFM parameters [27-28]. The experiments of all compounds with its different concentrations were conducting at 25 ± 0.1 °C.

2.3.4. Electrochemical Impedance Spectroscopy (EIS)

The circuit equivalent model consumed for this system where R_{ct}= resistance charge transfer and R_s= resistance of solution, and C_{dl}= double layer capacitance. EIS300 software that used for test of EIS. Echem Analysis 5.5 software was utilized for appropriate plotting.

3. Results and discussion

3.1. Characterization of ligand and complexes

3.1.1. Elemental and conductance measurements

The tridentate ONO type of H_2L and its metal chelate (**1-6**) were synthesized and characterized by various spectral techniques. The elemental analyses (Table 1) are consistent with 1 : 1 metal to ligand stoichiometry and accordingly, these complexes have the general formulae {[$ML(X)_2$]Y}(M = Cu(II)(**1**), Y = H_2O; Co(II)(**2**); Ni(II)(**3**), Mn(II)(**4**), X = H_2O, Y = nill; and M = Cd(II)(**5**), Y = 0.5 H_2O UO_2(II)(**6**); X = nill. All the complexes reported here are colored and stable towards air and moisture. The formed complexes are

insoluble in common organic solvents and sparingly soluble in coordinated solvents. The conductance measurements (25 ºC) in DMF are in accord with the non-electrolytic nature of the complexes.

TG analyses confirmed the presence of two molecules of coordinated water in the complexes (**1-5**).

The ligand H_2L may be exist in equilibrium mixtures of I, II; III, IV and/or V forms or may prefer only one of the forms (Fig. S1) depending upon the energy difference amongst these tautomeric forms.

3.1.2. Magnetic susceptibility values

The magnetic moment was measured at room temperature as shown in Table 1. The Cu(II) complex has magnetic moment value of 1.62 BM,. This low value of magnetic moment assign to the metal-metal interactions through the presence of bridging structure**.** The $\mu_{eff.}$ value of Co(II) complex is found to be 4.48 BM, suggesting the octahedral geometry [29-33]. Similarly Ni(II) and Mn(II) complexes have magnetic moment values 2.61 and 5.46 B.M., respectively, which suggest an octahedral geometry [33-35]. As UO_2(II) complex was diamagnetic, an octahedral geometry was also proposed for this complex referring to their elemental analysis and spectroscopic analytical data and their empirical formula [36-38].

3.1.3. Electronic spectral studies

The electronic spectrum of Schiff base (H_2L) exhibits three bands at 30100 (n-π*), 33100 (π-π*) and 34250 cm^{-1} (hydrogen bonding and association) [27,39,40]. The spectrum of complex (**5**) exhibited bands assigned to Schiff base π→π* and L→M charge transfer [38]. This complex is diamagnetic as expected. The metal normally prefers tetrahedral coordination. In the dioxouranium(VI) complex (**6**), the π-π* transition shifts to lower energy at ~ 28150 cm^{-1}, and the band due to the hydrogen bonding and association is absent as expected. The band due to π-π* transition moves to lower energy at ~ 31150 cm^{-1}. These shifts or disappearance of the bands are indicative of coordination of the Schiff base to UO_2^{2+}. The dioxouranium(VI) complex exhibits a new band at 23800 cm^{-1} which is assigned to the $^1\sum_g^+ \rightarrow {}^3\pi_u$ transition typical of OUO symmetric stretching frequency for the first excited state [36,37]. The υ_{as}(OUO, 885) and υ_s(OUO, 790 cm^{-1}) modes of the complex. The force constant, f_{U-O} was calculated by the method of McGlynnetal. [41] and the value (6.51 mdyne/Aº) is the expected range [37]. The bond length was calculated with the help of the equation, $R_{U-O} = 1.08f^{-1/3} + 1.17$. The U-O bond distance is 1.75 Aº which is in the usual range (1.60-1.92 Aº) observed for the majority of dioxouranium(IV) complexes [36].

In the UV-vis. spectra of the complexes, the azomethine chromophore π-π* transition is shifted to 23310—22120 cm^{-1}, indicates the coordination of imino nitrogen of the ligand to the metal ion. The absorption frequencies ascribed to the benzene π-π* transition are slightly changed as a result of the influence of the benzene ring on the coordination interaction [42].

The electronic spectral band at 15260 cm^{-1} corresponds to $^2E_g \rightarrow {}^2T_{2g}$, transition in Cu(II) complex**(1)**suggesting a distorted octahedral geometry.

The spectrum of complex (**2**) exhibits three electronic spectral bands 12980, 21750 and 26540 cm^{-1} transition in an octahedral field. The electronic spectral parameters of the complex are as follows [43-45]: Dq = 8770 cm^{-1}, LFSE (kcal mol^{-1}) = 251.17, B` = 623 cm^{-1}, β = 0.64, β_o = 36 %. The β^o value of 36 % testifies to the presence of strong M-L covalent bonding in the complex of the Racah parameter from the free ion value.

The complex (**3**) exhibit three bands at 12400, 19200 and 27900 cm^{-1} transitions suggesting the octahedral geometry [22,46]. The value of υ_2/υ_1 ratio (1.54) of Ni(II) complex supporting the octahedral structure [47]. The spectrum Rarach parameters of the Ni(II) complex as calculated according to the method of Lever [48] are as follows:

Dq = 12400 cm^{-1}, B` = 660 cm^{-1}, LFSE = 426.15 kcal mol^{-1}, β= 0.64, β^o = 36 %.The reduction of the Racah parameter and the β^o value of 36% are indicative of the presence of strong covalence in the complex.

The electronic spectrum of Mn(II) complex (**4**) show bands 18655 ($^6A_{1g} \rightarrow {}^4T_{1g}(^4G)$), 24650 ($^6A_{1g} \rightarrow {}^4E_g$, $^4A_{1g}$ (^4G)), 29410 ($^6A_{1g} \rightarrow {}^4E_g$, ($^4G$)) and 39370 cm^{-1} ($^6A_{1g} \rightarrow {}^4T_{1g}$, ($^4P$)) transitions depend only on the values of the Racah parameters B and C [49]. The experimental observed transition energies are used to calculate the values of parameters B(775), C(3374), Dq(854) and β(0.79). The value of Dq could be evaluated from a Tanabe-Sugano diagram for the d^5 system [50]. The Slater, Condon- shortly parameter F_2 (1255) and F_4 (95) have been calculated by using values of the Racah parameters B and C. The magnetic moment of complex under study at room temperature is 5.97 B.M., which are characteristic of distorted octahedral geometry.

3.1.4. ESR spectrum

The ESR spectrum of the Cu^{2+} chelate (**1**) displayed two g-values. The calculated values of $g_{||}$, $g_{\perp}$ and g_{av} are 2.288, 2.094 and 2.129, respectively. The g_{av} value has a positive contribution apart from that of the free electron (2.0023) due to the

reasonable covalent character in the bond between the ligand and Cu^{2+} ion (Table S1). The value of $g_{\|}$ being less than 2.3 denotes that the Cu^{2+} complex has covalent character. The trend $g_{\|} > g_{\perp} > 2.0023$ observed for this complex show that the unpaired electron is localized in d_{x2-y2} orbital of Cu(II), characteristic of tetragonally elongated structure for Cu(II) complex. The exchange interaction parameter between the Cu(II) centers in the polycrystalline compound is calculated by using the expression:

$$G = (g_{\|}-2.0023)/(g_{\perp}-2.0023),$$

The low value of G (3.12) which is less than 4, suggesting considerable interaction in the solid state [51]. ESR spectra of the complex were used to determine the elongated Cu(II) complex (D_{4h} symmetry), bonding parameters such as the unpaired electron in $3d^9$ case assigned to $3d_{x2-y2}$ orbital and the overlapping of this anti-bonding orbital with the ligand 2s and 2p σ orbital using of the following equation [15]:

$$\alpha^2 = A_{\|}/0.036 + (g_{\|}-2.0023) + 3/4(g_{\perp}-2.0023) + 0.04$$

where $\alpha^2$is the strength of the interaction between the metal and the ligands. α^2 value was found to be 0.72.which is less than unity. Therefore, the complex has covalent character [52]. Also, as shown in Table S1, α^2 is less than β^2 (0.91) inferring the presence of covalency in the in-plane π bonding than the in-plane σ bonding. The f (174) value suggest highly distorted structure for the Cu(II) complex is suggested.

3.1.5. Infrared spectroscopic study

The IR spectrum of the Schiff base ligand (H_2L) (Fig. S2) showed the appearance of a strong new band at ~ 1624 cm^{-1}assigned to the azomethine υ(CN) linkage. The absence of bands at 1734 and 3420 cm^{-1} due to carbonyl υ(CO) and υ(NH_2) stretching vibrations suggesting that the amino and aldehyde moieties of the starting reagents are absent and have been converted into the azomethine moiety (Fig. S1).

The active site of the ligand and their bonding to the metal ions was characterized by careful comparison of the main infrared absorption bands of the free ligand and its complexes are shown in Table 2. FT-IR spectra of all complexes show that H_2L behaves as monobasic tridentate ligand, corresponding *via* (CN), and two phenolic (O-H) oxygen groups. Also, two intense bands observed to 1624 (CN) and 1460 cm^{-1} (C-O).

The ^{1}H NMR (DMSO-d_6) (Fig. S3) and ^{13}C NMR (Fig. S4) data of the Schiff base ligand (H_2L) are presented in Table 3. In general, the duplets or triplet peaks observed at 6.80-8.40 ppm are assigned to naphtholic and aromatic ring protons. The singlet peaks at 9.50, 10.35 and 15.65 ppm are assigned to imine, aromatic and naphtholic hydroxyl protons, respectively. The signals of OH groups lying at higher field side can be attribute to the contribution of the OH groups intramolecular and intermolecular hydrogen bonds (Fig. S1). Addition of D_2O to the previous solution shows the absence of the last two signals due to proton exchange (Fig. S3). The ^{1}H NMR spectra of complexes (**5** & **6**) were recorded in DMSO-d_6 (Table 3 and Figs. S5 & S6). The signals due to the phenolic and naphtholic hydroxyl protons groups are also absent in the spectra of complexes indicating the coordination of the phenolic oxygens atoms to the metal ions. The downward shift of the azomethine proton signal in the complexes indicates the coordination of the azomethine nitrogen [37,53]. Thus, the ^{1}H NMR data indicate tridentate and dibasic nature of the Schiff base. The ^{13}C NMR spectra data of the H_2L (Table 3 & Fig. S4) are in accord with the proposed structures. The ^{13}C NMR spectra of H_2L shows a peak at 178 ppm which may be assigned to the CH=N group. The spectrum of the ligand shows a cluster of peaks in the region 106-150 ppm due to aromatic carbons (C-H).

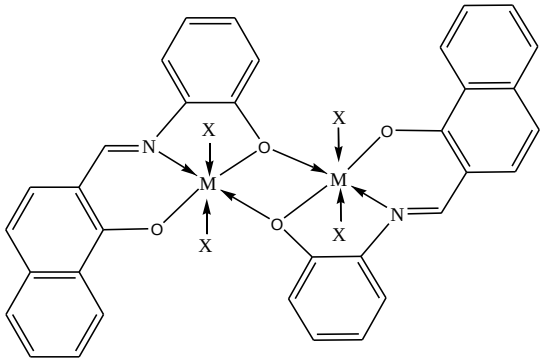

M = Cu(II)(1), Co(II) (2), Ni(II) (**3**), Mn(II) (**4**); X = H_2O

= Cd(II) (**5**), UO_2(II) (**6**); X = nil

Fig. 1. Supposed structure of the complexes.

Table 1. Analytical data of Schiff base ligand **(H_2L)** and its complexes

Comp.[a]	Expt. (calcd.) %				$\mu_{eff.}$
	C	H	N	M	**(B.M.)**
H_2L	80.17 (80.25)	4.88 (4.93)	5.74 (5.91)	-	-
(1)	53.78 (53.89)	3.85 (3.96)	3.54 (3.70)	16.55 (16.79)	**1.90***
(2)	57.12 (57.32)	4.17 (4.26)	3.79 (4.14)	16.39 (16.56)	**5.04**
(3)	57.29 (57.35)	4.12 (4.2)	3.74 (3.94)	16.33 (16.50)	**3.31**
(4)	57.83 (57.96)	4.17 (4.26)	2.88 (3.98)	15.44 (15.61)	**5.97**
(5)	53.22 (53.35)	2.68 (2.88)	3.49 (3.66)	29.15 (29.39)	**Dia.**
(6)	38.21 (38.42)	1.98 (2.07)	2.46 (2.64)	44.56 (44.82)	**Dia.**

[a]Numbers as given in Fig. 1. *The magnetic moment of the copper(II) complex calculated using the relation $\mu^2 = 3/4\ lgl^2$ is 1.87 B.M.

The mass spectrum of the Schiff base ligand (H_2L) exhibits a parent molecular ion peak at m/z = 263amu corresponding to the weight formula of the ligand [$C_{17}H_{13}NO_2$]. The peak at m/z 169 amu is due to ligand (H_2L) after the removal of C_6H_6O atoms as shown in Scheme 1. This fragment undergoes further fragmentation by the removal of C_2H_3NO atoms giving molecular ion peak at m/z = 113amurepresent C_9H_4fragment. The spectrum shows molecular ion peak at m/z = 76 amu corresponding to the C_6H_4 fragment. The information gathered from mass spectrum data agrees well with elemental analyses.

The electron impact mass spectra of Cu(II) complex **(1),** Co(II) complex **(2)** and Mn(II) complex **(4)** are shown in Schemes 2-4. The molecular ion peak of m/z = 378.54 amu undergoes fragmentation to a stable peak at m/z = 280.54, 230.54, 151 and 125 amu by losing $3H_2O + C_2H_4O$, C_4H_2, CuO and CN atoms, respectively, for Cu(II) complex **(1)** (Scheme 2).

For Co(II) complex **(2)**,the molecular ion peak of m/z = 355.93 amu undergoes fragmentation to a stable peak ions at m/z = 302.93, 244, 152, 100 and 76 amu by losing $2H_2O$ + OH, Co, C_6H_4O, C_3H_2N and C_2 atoms, respectively (Scheme 3).

The molecular ion peak at m/z = 351.94 amu for Mn(II) complex **(4)** undergoes fragmentation to a stable peak at m/z = 313.94, 263.94, 169, 139, 115 and 65 amu by losing $2H_2O + H_2$, C_4H_2, C_2MnO, NO,C_2 and C_4H_2 atoms, respectively (Scheme 4).

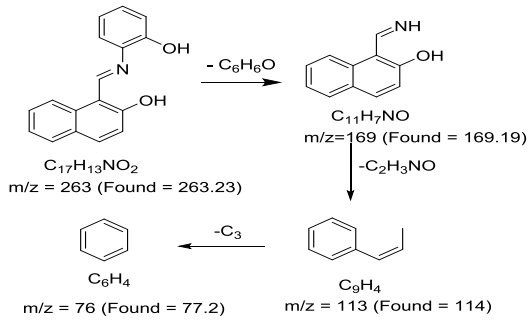

Scheme 1. The fragmentation patterns of mass spectrum of ligand (H_2L).

FT-IR spectrum for ligand H_2L, displayed a two bands at (3480 and 3361cm^{-1}) may due to interference of the phenolic OH groups [54]. On the other hand, the spectrum displayed band of weak intensity at 3221 cm^{-1}, this band may due to intramolecular hydrogen bonding (OH…N) group [55,56]. In the spectra of the complexes, these absorption bands disappears and strong band of υ(C-O) in the Schiff base is resolved into two peaks in the complexes, the first is lower energy to υ(C-O) (naphthanolic moiety)(1342-1388cm^{-1}), while the second is higher energy υ(C-O, benzene moiety)(1492-1499cm^{-1}) [57]. Both the bands occur at higher frequencies compared to υ(C-O) in the free H_2L. This indicates participation of both the phenolic oxygen in coordination subsequent to deprotonation [58]. The displacement of these bands to higher frequencies is attributed to the increase in the bond strength of C-O on extended delocalization of the system of the naphtholidene moiety. The dimeric nature of the complexes is also supported by the appearance of new bands at ~740-749 cm^{-1}.

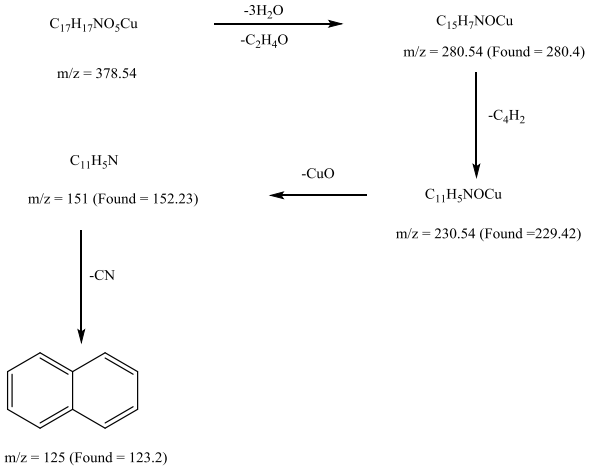

Scheme 2. The fragmentation patterns of mass spectrum of complex **(1)**.

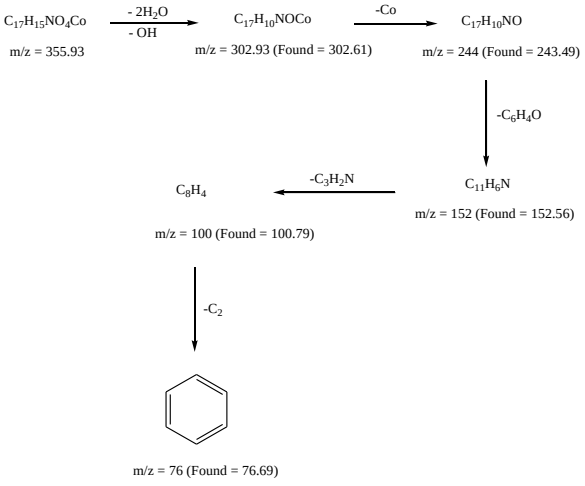

Scheme 3. The fragmentation patterns of mass spectrum of complex **(2)**.

The band at 1624 cm^{-1}indicate the appearance of imine (C=N) band, which reveals the formation of Schiff base ligand [30,37]. In the FT-IR spectra of the complexes the imine (C=N) band shifted to lower frequency and appeared at 1600-1627 cm^{-1} for complexes (**1-6**). The shift to lower or higher frequency can be attributed to the participation of the iminic nitrogen atom in the coordination to the metal [30,37]. This can be explained by the movement of electrons from the iminic nitrogen to the metal ion (delocalization of metal electron density into the ligand π-system) as a result of coordination process, attributed to stretching of (C=N) imine group [30,37]. The presence of coordinated water molecules in all the complexes is indicated by a sharp band at ~3410 - 3471 cm^{-1} and two weaker bands at ~885 and 725 cm^{-1}, which could be assigned to OH stretching, rocking and wagging vibration, respectively. Finally, the spectra showed new bands at ~ (528.0-567.0), (450.8-475) and (510-555) cm^{-1} can be referred to $\upsilon(M–O)_{ar}$, $\upsilon(M\text{-}N)$ and $\upsilon(M–O)_{naphtha}$ for complexes, respectively. These new bands confirmed the coordination of the ligand to the metal ion through imine nitrogen and phenolic oxygen atoms [30].

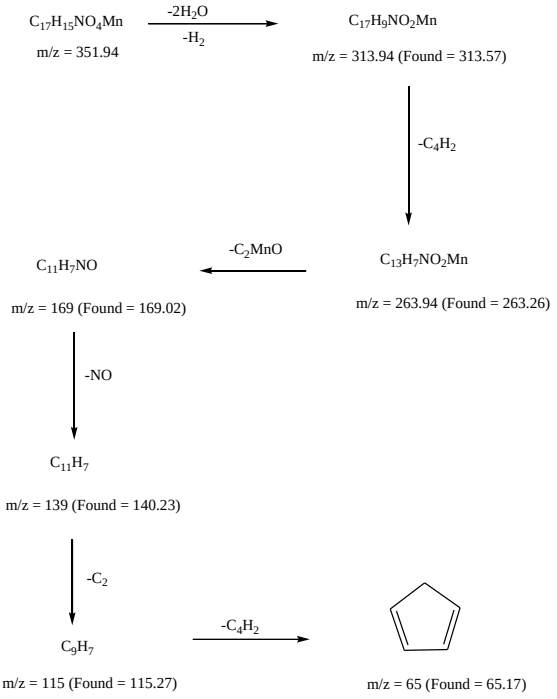

Scheme 4. The fragmentation patterns of mass spectrum of complex **(4)**.

According to Karagonius and Pete [60] and EI-Sonbati, [61], the distance between the metal ion and the coordinated center of the organic ligand is the main factor affecting the IR band shifts. The coordination band length was determined from the relation [59-61]:

$\Delta\upsilon = (32\pi\alpha/a^2)\,[(\upsilon_{x=y} - \upsilon_{x\text{-}y})/L]\,\exp[-2\pi(2r/a)^{1/2}]$

where $\Delta\upsilon$ is the shift in the oscillator frequency (ν_{ligand}- $\nu_{complex}$); α is the bond polarizability; a is the lattice constant of the used metal salt; $\nu_{x\text{-}y}$ is the frequency of the oscillator with a single bond, $\nu_{x=y}$ is the frequency of the oscillator with a double bond; and L is the length of the oscillator coordinated to the metal ion. The calculated coordination bond lengths of the Cu(II), Co(II) and Ni(II) are in the

following sequence: Cu(II)(3.082 Aº) < Co(II)(3.195Aº) < Ni(II)(3.230 Aº) .

Furthermore, it was found that the frequency values of the M-N decrease in the same order as the azomethine frequencies, suggesting that the strength of the metal-nitrogen bond is in the same decreasing order. It seems that the greater strength of the electrostatic field of the copper and accordingly the smaller ionic radius of the Cu(II) ion than that of either Ni(II) or Co(II) ions is the main reason of shorter coordination bond lengths for the copper complexes. In addition the greater number of d-electrons in Cu(II) ions than either Ni(II) or Co(II) ions.

3.2. X-Ray diffraction analysis

The X-ray diffraction (XRD) patterns of the Schiff base ligand (H_2L) and its complexes **(1, 3** and **4)** powder are shown in Figs. 2-5. The XRD patterns show many diffraction peaks which indicate the polycrystalline phase. The determined lattice parameters (a, b, c, α, β and γ) and Miller indices (hkl) for H_2L and its complexes **(1, 3** and **4)** are listed in Tables S2-S5.

3.3. Thermogravimetric analysis (TGA) and kinetic studies

The thermogravimetric analyses (TGA) of ligand (H_2L) and its Cu(II), Co(II), Ni(II), Mn(II) and UO_2(II) complexes are shown in Fig. 6 and the loss of mass percentages were summarized in Table 4.

Horowitz–Metzger and Coast–Redfern methods [62,63] were used for the determination of the values of activation energy (E_a), enthalpy (ΔH), entropy (ΔS) and Gibbs free energy (ΔG) of the decomposition of the ligand (H_2L) and its complexes(**1-4** and **6**) were determined graphically as shown in Figs. S7, S8 and Table 5. It was found that the value of E_a of H_2L is higher than all the prepared complexes and the complex **(3)** have higher E_a than the other complexes. This can be attributed to the loss of water molecules in the complexes [33,64]. Therefore, the order of stability for the complexes is:

H_2L > **(3)** > **(4)** > **(6)** > **(1)** > **(2)**.

The negative ΔS^* values for the decomposition steps indicate that all studied complexes are more ordered in their activated state [33,44]. The highest value of E_a for Ni(II) complex **(3)** than the other complexes may be due to the lower ionic radius of Ni(II) in comparison to the other studied ions.

Table 2. Important Infrared spectra peaks (cm^{-1}) of H_2L and its complexes.

Compound[a]	υ(OH)	υ(C=N)	υ(C-O)	$\upsilon(M\text{-}O)_{ar}$	υ(M-N)	$\upsilon(M\text{-}O)_{naph.}$
H_2L	3480, 3361,3221	1624	1460	-	-	-
(**1**)	-	1604	1492	533	472	550
(**2**)	-	1607	1494	540	465	540
(**3**)	-	1607	1492	545	460	535
(**4**)	-	1620	1499	554	456	525
(**5**)	-	1627	1496	565	453	518
(**6**)	-	1627	1498	558	450	512

[a]Numbers as given in Table 1.

Table 3. ^{1}H NMR and ^{13}C NMR chemical shift (ppm) of Schiff base (H_2L) and its complexes (**5** & **6**).

Compound[a]	**^{1}H &^{13}C NMR (400 MHz DMSO/TMS: δ ppm)**
H_2L 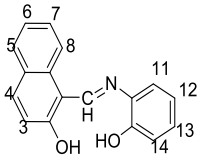	6.80(d, 1H, H-3), 6.95(t, 1H, H-6), 7.05(t, 1H, H-7), 7.15 (t, 1H, H-8), 7.28(t, 1H, H-5), 7.48(t, 1H, H-4), 7.68(d, 1H, H-11), 7.80(d, 1H, H-12), 7.85(d, 1H, H-14), 8.40(d, 1H, H-13), 9.50(s, 1H, CH=N), 10.35(s, 1H, Ar.-OH), 15.75(s, 1H, naphtholic ring-OH).
	106, 116, 118, 120, 123, 126, 127, 128, 129, 130, 134, 138, 149, 159
(5)	Azomethineproton, 9.50 Aromatic protons, 6.75-8.28
(6)	Azomethineproton, 9.41 Aromatic protons, 6.55-8.35

[a]Numbers as given in Table 1.

Table 4. TGA thermal data of **(**H_2L) ligand and its complexes.

Compound[a]	Temperature range (°C)	TG weight loss %		Assignments
		Found	Calc.	
Ligand	220-320	14.80	14.83	C_3H_3
	320-800	4.80	4.94	CH
	> 800	80.40	80.23	$C_{13}H_9NO_2$
(1)	40-100	4.60	4.76	H_2O
	100-700	74.50	74.23	$2H_2O + C_{17}H_{11}NO$
	> 700	20.90	21.01	CuO
(2)	35-150	10.20	10.12	$2H_2O$
	150-800	58.50	58.72	$C_{14}H_{11}NO$
	> 800	31.30	31.16	CoO + 3C
(3)	65-185	10.32	10.12	$2H_2O$
	185-700	68.66	68.89	$C_{17}H_{11}NO$
	> 700	21.02	20.99	NiO
(4)	70-375	18.90	18.75	$2H_2O + CH_2O$
	375-500	17.08	17.90	C_5H_3
	500-600	18.33	18.19	C_5H_4
	600-800	11.20	11.36	C_2H_2N
	> 800	34.49	33.80	MnO + 4C
(5)	45-300	9.66	9.79	C_4H_4
	300-360	7.28	7.17	C_3H_2
	360-462	10.06	10.16	C_3H_2O
	462-700	22.38	22.03	C_7H_3NO
	> 700	50.62	50.85	UO_2

[a]Numbers as given in Table 1.

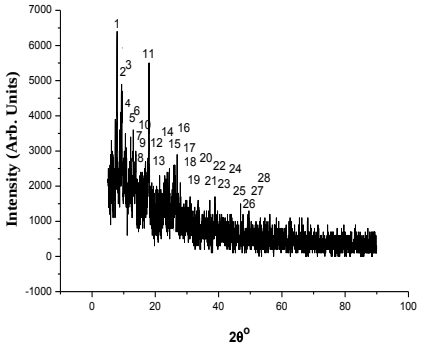

Fig. 2. The XRD pattern of ligand (H_2L).

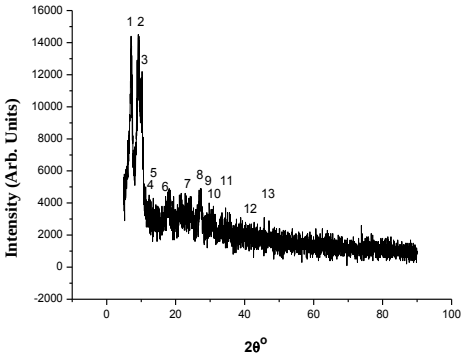

Fig. 3. The XRD pattern of complex **(1)**.

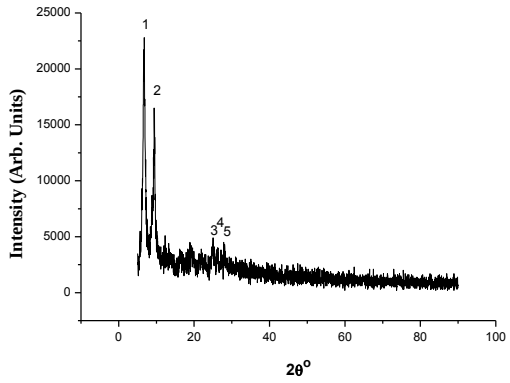

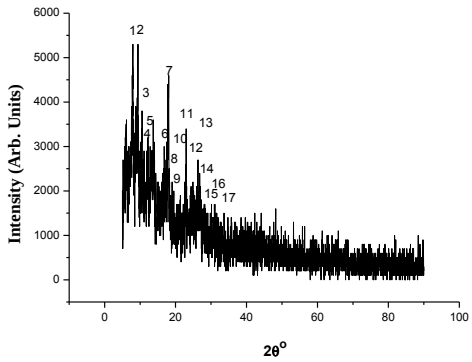

Fig. 4. The XRD pattern of complex **(3)**. **Fig. 5.** The XRD pattern of complex **(4).**

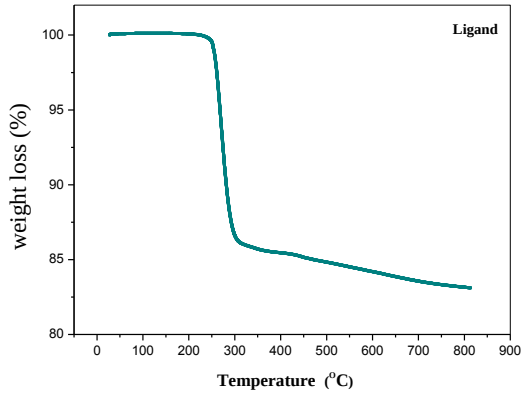

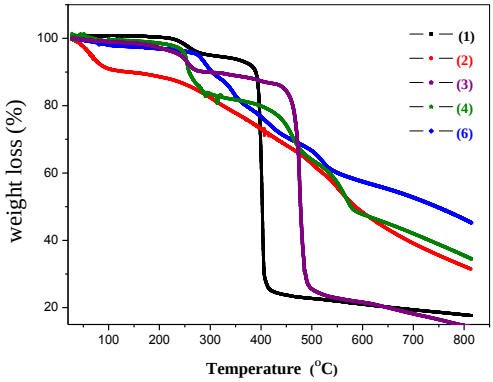

Fig. 6. TG curves of ligand and its polymer complexes **(1, 2, 3, 4 and 6)**.

3.4. Biological analysis

The tested bacteria and fungi that we used in our assay were recognized as dangerous food borne pathogens which can be transmitted to our food by many ways of contamination; during packaging, polluted water, poor hygiene and contaminated tools. Food diseases or food spoilage are the widespread health problems and a major cause of the reduction in economic productivity and human lives around the world [65].

Different amounts of antimicrobial inhibition against pathogenic bacteria and fungi were obtained by varying the concentrations of the prepared compounds. The measured growth inhibition zone (a Kirby-Bauer Test)ranging from 10 to 30 mm for all the sensitive bacteria and ranging from 10 to 26 mm for all the sensitive fungi [66]. From Tables 6 and 7, it was found that the antibacterial activities of all tested compounds increased linearly with the increase in the concentration of extracts. Concentrations of 50, 100 and 150 µg/mL of exhibits provide a strong antibacterial activity against Gram-positive bacteria (*Staphylococcus aureus* and *Bacillus subtilis*) comparing to Gram-negative bacteria (*Pseudomonas aeruginosa*, *Klebsiella pneumoniae* and *Escherichia coli*). These results are in agreement with the results suggested by Abou-Dobara et al. [19].

Inhibition zone of complex **(3)** against *Staphylococcus aureus*was 30 mm while its inhibition zone against *Klebsiella pneumoniae* was 17 mm only at 150 µg/mL. Ligand and its complexes **(1, 2, 4** and **6)**have not any antibacterial effect against *Klebsiella pneumoniae* and low activity against *Pseudomonas aeruginosa*, while they have great antibacterial activity against other tested Gram positive bacteria. These resistant of Gram negative bacteria due to their structure of the cell wall which have a largely impermeable wall which excludes drugs and antimicrobial compounds from penetration the cell, The outer membrane of Gram negative bacteria contains hydrophilic lipopolysaccharides (LPS), which creates a barrier toward macromolecules [67,68], in contrast for Gram positive cell wall which has thick porous peptidoglycan allowed for antimicrobial compounds to penetrate the cells and showed its effect [69]. This result was agreed with Kim et al. [70].

Table 5. Thermodynamic data of the thermal decomposition of ligand **(**H_2L) and its complexes.

Compound[a]	Decomposition temperature (°C)	Method	Thermodynamic parameters				Correlation coefficient
			E_a (kJ mol^{-1})	ΔS^* (J mol^{-1} K^{-1})	ΔH^* (kJ mol^{-1})	ΔG^* (kJ mol^{-1})	
Ligand	246-316	CR	117	-104	113	170	0.96206
		HM	106	-100	101	157	0.96335
(1)	381-418	CR	99.7	-163	94.2	204	0.97464
		HM	88.1	-167	82.5	195	0.97230
(2)	240-653	CR	44.8	-246	38.8	216	0.98309
		HM	40.7	-249	34.7	214	0.97766
(3)	438-499	CR	130	-119	124	212	0.99533
		HM	126	-127	120	214	0.99479
(4)	390-481	CR	115	-121	109	195	0.99602
		HM	112	-139	106	205	0.99612
(5)	272-325	CR	100	-120	95.4	164	0.96268
		HM	93.9	-129	89.1	163	0.96209

[a]Numbers as given in Table 1

The concentration of 150 µg/mL showed the highest effect against all bacterial species. Although *Bacillus subtilis* showed resistant to many types of standard antibiotics such as Amoxicillin (10 µg/disk), Ampicillin (10 µg/disk), Streptomycin (10 µg/disk), Gentamicin (10 µg/disk) and Chloramphenicol (30 µg/disk)) [71,72], this resistance of *Bacillus subtilis* due to its ability to forming resistant endospore, also it has mutant resistant gene to antibiotics during its vegetative growth [72], but in this research all

synthetic compounds were have great antibacterial effect against *Bacillus subtilis.* The ligand showed lowest antimicrobial activity (5 – 7 mm) at 150 µg/mL concentration against all tested bacteria comparing to the activity of other synthetic compounds except complex **(6)** against *Klebsiella pneumoniae* and *Escherichia coli* and ligand against *Escherichia coli*, complex **(3)** against *Pseudomonas aeruginosa* and ligand and its complexes **(1, 2** and **4)** against *Klebsiella pneumoniae* which has not any antibacterial effect.

Most of the antibiotics are targeted to the intracellular processes, i.e., to show their effects they must be able to penetrate the bacterial cell, so the ability of compound to causing antimicrobial effect against microorganism depending on the size of its molecules and the structure of cell wall's microorganism in addition to the size of its pores which allowed to enter the molecule inside the cell and cause its effect or not, the outer membrane in Gram negative bacteria, which excludes certain drugs and antibiotics from penetrating the cell, but Gram positive bacteria do not have outer membrane, so they are more susceptible to antimicrobial compounds, The porn channels in Gram negative bacterial outer membrane prevent the entry of relatively large molecules, in addition to the Gram-negative bacteria have a high transformation rate, i.e., they have a great facility for exchanging genetic material (DNA) among strains of the same species and even among different species.

This means that if a Gram -negative bacterium either undergoes a genetic change (mutation) or acquires genetic material that confers resistance to an antibiotic [73], that is explained our data which most of Gram negative bacteria are more resistant toward the tested synthetic compounds than the Gram positive bacteria which have porous cell wall and antimicrobial molecules can enter inside it easily. When we used Penicillin as standard drug against the tested bacteria and compared as antibacterial effect with the synthetic compounds, we found that; all synthetic compounds showed stronger antibacterial activity than penicillin.

For the effect of synthesized compounds on the tested fungi; we found that the antifungal activity of these compounds is lower than its antibacterial activity. There is not any antifungal activity against all tested fungi except A. niger (Table 8). These may due to the complex structure of fungal cells more than the bacterial cells, composed of manly polysaccharides, can promote entering these molecules inside the fungal cells and cause inhibition, the cell wall of fungi not play role in keeping the morphology of cells but also protect cells from extracellular stress and antifungal substances [74].

The data showed that the antifungal effect of ligand against *A. niger*. Similar effect was observed with the complexes **(2, 4, 5** and **6)** where the inhibition zone ranged from (23-26 mm) at 150 µg/mL concentrations, but the ligand has antifungal effect

less than its complexes **(1** and **3)**, in addition to the standard tested antifungal compound (Miconazole). *Aspergillus niger* is filamentous mycotoxin producer fungus which has hazard effect on human health [74].

Table 6. Antibacterial activities of different synthesized compounds against two Gram positive pathogenic bacteria test organism (mean ± SD)

Compound[a]	Concentration (µg/mL)	Width of inhibition zone (mm)	
		S. aureus	***B. subtilis***
Ligand (H_2L)	**50**	8±.01	11±.01
	100	9±.01	12±.02
	150	10±.02	13±0
(1)	**50**	19±.01	16±0
	100	20±.07	17±0
	150	23±.01	19±0
(2)	**50**	18±0	13±.01
	100	19±0	15±.02
	150	20±0	17±0
(3)	**50**	22±.01	10±.01
	100	25±.04	14±.06
	150	30±.03	15±.02
(4)	**50**	13±.01	8±.01
	100	15±.02	14±.02
	150	18±.02	16±.03
(5)	**50**	20±.02	15±.01
	100	22±.03	20±0
	150	25±0	22±0
(6)	**50**	20±0.13	15±0.01
	100	25±0.12	16±0
	150	30±0.1	17±0
Penicillin	**50**	2±0	0
	100	3±0.1	0
	150	4±0.1	0

[a]Numbers as given in Table 1.

Table 7. Antibacterial activities of different synthesized compounds against three Gram negative pathogenic bacteria test organism (mean ± SD)

Compound[a]	Concentration (µg/mL)	Width of inhibition zone (mm)		
		K. pneumoniae	***E. coli***	***P. aeruginosa***
Ligand (H_2L)	**50**	0	0	0
	100	0	0	10±0.1
	150	0	0	12±0.1
(1)	**50**	0	8±0	11±0
	100	0	13±0	14±.03
	150	0	15±0	15±.02
(2)	**50**	0	15±0	9±0.1
	100	0	16±0	10±0.1
	150	0	17±0	14±0.1
(3)	**50**	11±0	12±.01	0
	100	15±0	13±0	0
	150	17±0	14±.02	0

(4)	**50**	0	18±.05	13±0
	100	0	20±.03	15±0
	150	0	23±.06	16±0
(5)	**50**	11±0.1	11±0.03	8±0.09
	100	17±0	15±0	10±0.01
	150	20±0.2	19±0	13±0.04
(6)	**50**	0	0	8±0.04
	100	0	0	10±0.04
	150	0	0	12±0
Penicillin	**50**	0	2±0	1±0
	100	0	3±0.1	2±0
	150	0	4±0	3±0

[a]Numbers as given in Table 1.

Our data proved that *A. niger* was sensitive fungus toward the tested synthesized compounds more than other fungus, and that agreed with previous studies by El-Fatimi et al**.** [75].These synthetic substances were toxic to spores germination of *A. niger* which effect on the fungal cells by inhibition some series of physiological process and blocking the function of enzymes [76]. The higher concentrations of the synthesized compounds were needed to kill the fungal cells to inhibit the growth of these cells on time-kill profile study [77,78]. According to the statistical analysis, all tested fungi were significantly affected by compound differences (with higher F ratio) more than that of a concentration for all fungal species.

3.5. Molecular docking of the ligand

Molecular docking has been studied between Schiff base ligand (H_2L) and two types of proteins namely *Escherichia coli* (3t88) and *Staphylococcus aureus* (3q8u) [15]. The docking studies show an acceptable interaction between H_2L and the receptors of each protein as showed in Figs. 7 and 8. Figures 9 and 10 show HB plot curves due to the binding of the ligand to the proteins by hydrogen bonding interactions [79,80]. The calculated binding energy values are presented in Table 9. The estimated free energy of binding (kcal/mol) is -6.82 and -5.90 for the receptors of *Staphylococcus aureus* (3q8u) and *Escherichia coli* (3t88), respectively. The interact surface value is 663.782 and 548.082 for the receptors of *Staphylococcus aureus* (3q8u) and *Escherichia coli* (3t88), respectively. 2D and HB plot curves of molecular docking with H_2L are shown in Figs. 11 and 12. From Table 9, the value of estimated free energy of binding (kcal/mol) indicated that the Schiff base ligand (H_2L) is higher and stronger inhibitory activity against receptor target. According to the results showed in Table 9, the receptor of *Staphylococcus aureu* (3q8u) shows the best interaction than the receptor of *Escherichia coli* (3t88) with the H_2L.

Table 8. Antifungal activities of different compounds against fungal test organism (mean ± SD).

Compound[a]	**Concentration (µg/mL)**	**Width of inhibition zone (mm)**			
		A. niger	***A. alternate***	***F. oxysporum***	***C. albicans***
Ligand (H_2L)	**50**	15±0.06	0	0	0
	100	16±0.05	0	0	0
	150	18±0.01	0	0	0
(1)	**50**	13±0.02	0	0	0
	100	14±0.02	0	0	0
	150	15±0.01	0	0	0
(2)	**50**	20±0	0	0	0
	100	22±0	0	0	0
	150	25±0	0	0	0
(3)	**50**	12±0.03	0	0	0
	100	15±0.02	0	0	0
	150	17±0	0	0	0

(4)	**50**	19±0.04	0	0	0
	100	20±0.02	0	0	0
	150	23±0.01	0	0	0
(5)	**50**	18±0.06	0	0	0
	100	21±0.02	0	0	0
	150	26±0.	0	0	0
(6)	**50**	17±0.01	0	0	0
	100	19±0.02	0	0	0
	150	23±0.01	0	0	0
Miconazole	**50**	1±0	0	2±0.1	1±0
	100	3±0	0	3±0.1	1±0
	150	4±0.1	0	3±0.1	2±0.1

[a]Numbers as given in Table 1.

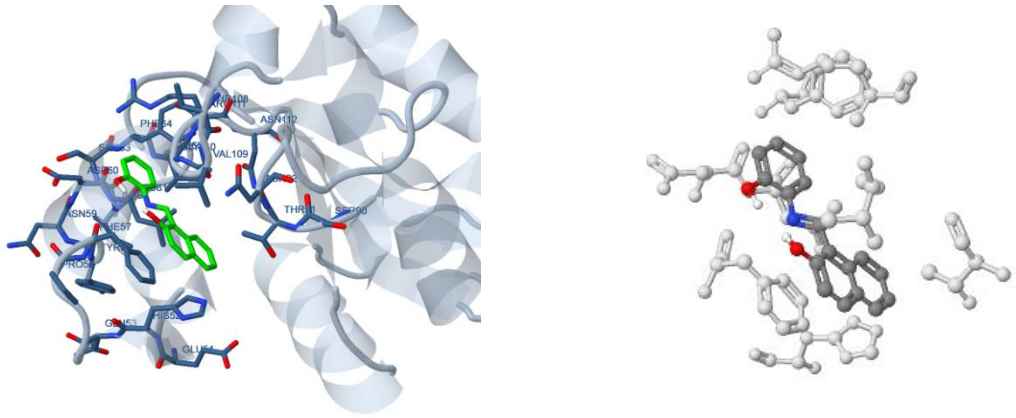

(a) (b)

Fig. 7. The ligand (green in (a) and gray in (b)) in interaction with receptor of *Staphylococcus aureus* (3q8u).

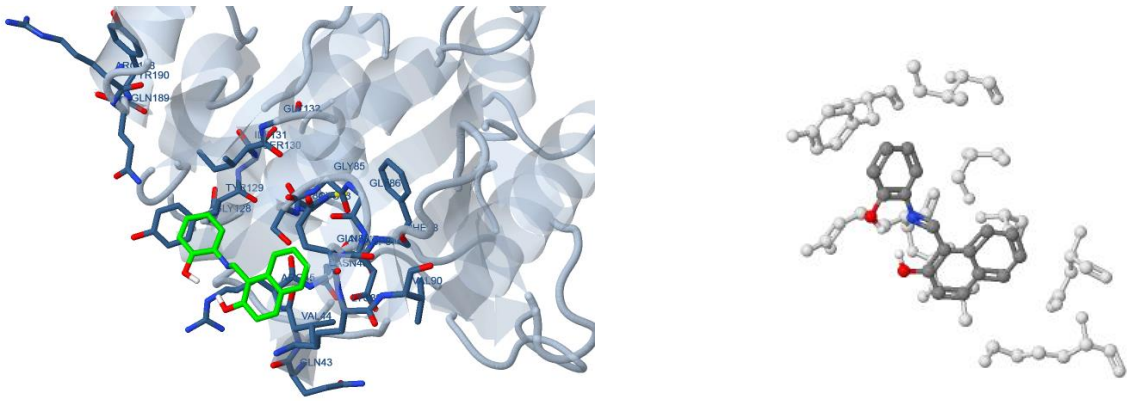

(a) (b)

Fig. 8. The ligand (green in (a) and gray in (b)) in interaction with receptor of *Escherichia coli* (3t88).

Table 9. The values of energy obtained in docking calculations of **(H_2L)** ligand with receptors of *Staphylococcus aureus* (3q8u) and *Escherichia coli* (3t88).

Receptor	Est. inhibition constant (K_i) (μM)	vdW+ bond+ desolv energy (kcal/mol)	Electrostatic Energy (kcal/mol)	Total intercooled Energy (kcal/mol)
3q8u	10.04	-6.76	+0.08	-6.69
3t88	47.51	-5.62	-0.02	-5.64

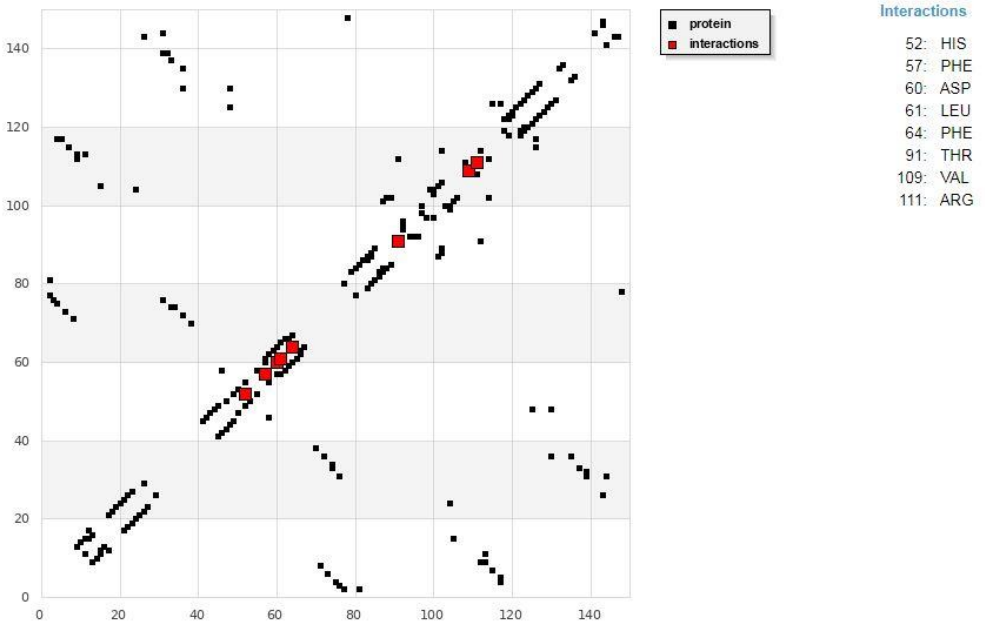

Fig. 9. HB plot of interaction between ligand and receptor of *Staphylococcus aureus*(3q8u).

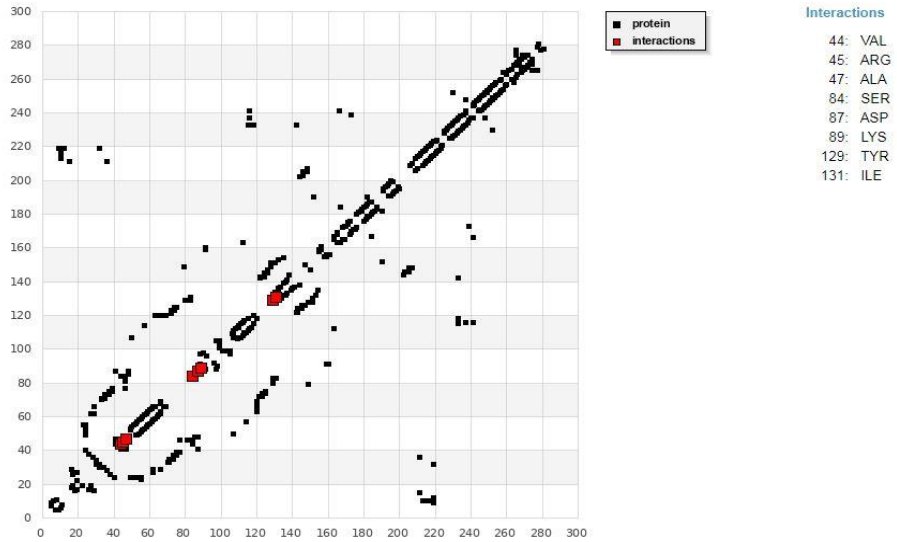

Fig. 10. HB plot of interaction between ligand and receptor of *Escherichia coli* (3t88).

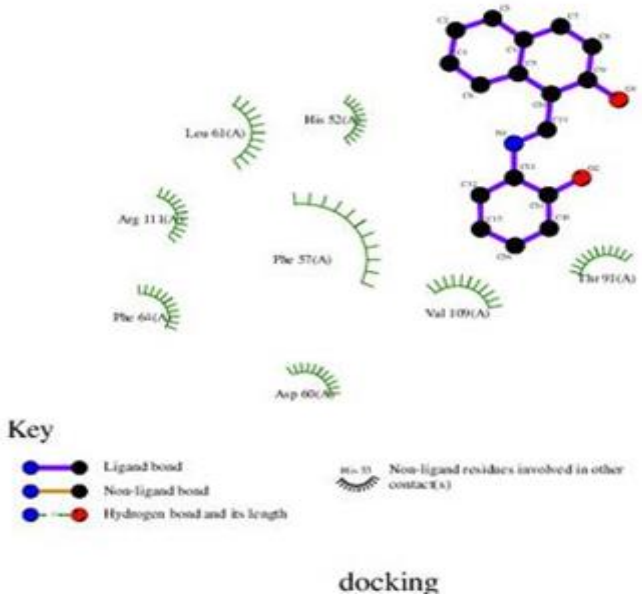

Fig. 11. 2D plot of interaction between ligand and receptor of *Staphylococcus aureus*(3q8u).

3.6. TP tests

The outcome of Schiff base ligand (H_2L) on the reactions by corrosion was examine by TP test. The exchanges in the TP diagram after the appending of H_2L is usually employed as the criteria to order inhibitor as anodic, cathodic or mixed [81]. Fig. 13 displays the Tafel diagrams forsteel-reinforced concrete for numerous concentrations of H_2L at 25 ± 0.1 °C. The Figure indicates that the cathodic plots give about parallel lines, signifying that the hydrogen discharge reaction depresses, its activation being controlled [82] by appending H_2L in HCl solution. The kinetic parameters were gained from Tafel plots and are presented in Table 10. The outcome data indicated that the appending of H_2L at all the planned concentrations resulted in:

i) A lower in the rate of corrosion and hence a breakdown in the current gotten from corrosion (i_{corr}),

ii) An development on θ and hence an increase in the % IE_p. There was no detected change in the corrosion potential (E_{corr}) value with blank. The % IE_p was determine using the following equation:

$$\%IE_p = [(i^o_{corr} – i_{corr}) / i^o_{corr}] \times 100$$

Where i^o_{corr} and i_{corr} = current corrosion existence and lack of H_2L, correspondingly.

3.7. EFM tests

Fig. 14 shows EFM spectra for steel-reinforced concrete attendance and lack of unlike concentrations of H_2Lat 25 ± 0.1 °C. The investigational EFM data were process exploited two various models [83]: "complete diffusion control of the cathodic reaction and the activation model. For the latter, a set of three non-linear equations had been solved, assuming that the corrosion potential concentration not change due to the polarization of the working electrode" [84].The parameters from EFM are represented in Table 11. The % IE raises by growing the investigated concentration of inhibitor. The causality factors (CF-2 and CF-3) are near to their theoretical value, viewing that the measured data are excellence good. The %IE and was obtain from the equation.

$$\% IE_{EFM} = [1-(i_{corr}/ i^o_{corr})] \times 100$$

Where i^o_{corr} and i_{corr}= current corrosion existence and lack of H_2L, correspondingly.

3.8. EIS tests

EIS is powerful and well-established technique in the procedure of corrosion [85-89]. Fig. 15 demonstrates the (a) Nyquist and (b) Bode curves obtain from OCP existence and nonexistence improving concentrations of compound (H_2L) at 25 ± 0.1 °C. The growth in the size of the loop capacitive with the appending of compound (H_2L) lead to a barrier progressively forms on the surface of steel-reinforced concrete. The difference from ideal semicircle was usually, led to the scattering of frequency [90] EIS spectra of the compound (H_2L) appending were calculated employed the circuit equivalent, Fig. 16, which signifies a single charge transfer reaction and fits well with our investigational data [91]. C_{dl}, for a

circuit containing a CPE parameter (Y_0 and n) were determining from Eq. [92]:

$$C_{dl} = Y_0\omega^{n-1}/ \sin [n (\pi/2)]$$

whereY_0 = magnitude of the CPE, $\omega = 2\pi f_{max}$, f_{max} = the frequency at which the imaginary of EIS is greatest. After experimental the Nyquist diagrams for corrosion procedure was mainly controlled on charged-transfer [93,94].

The outcome data gotten from EIS listed in Table 12 show that the R_{ct} improve and the C_{dl} data little with improve the compound (H_2L) concentrations. This is due to the regular replacement water molecules by the adsorption of the compound (H_2L) molecules on the surface of steel-reinforced concrete, depressing the extent of dissolution reaction [95,96]. The % IE was gotten from Eq. (4) [97-99]:

$$\% E = \theta \times 100 = [1-(R^{\circ}_{ct}/R_{ct})]$$

where, R^{o}_{ct} and R_{ct} are the resistance in the absence and attendance of compound (H_2L), correspondingly.

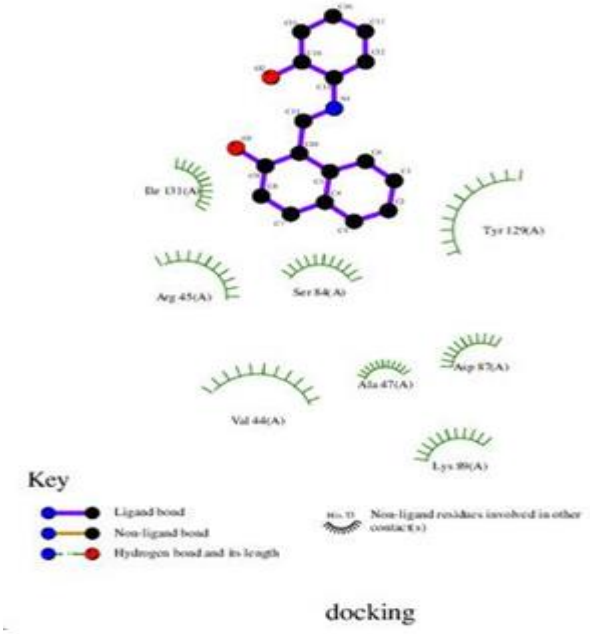

Fig. 12. 2D plot of interaction between ligand and receptor of *Escherichia coli* (3t88).

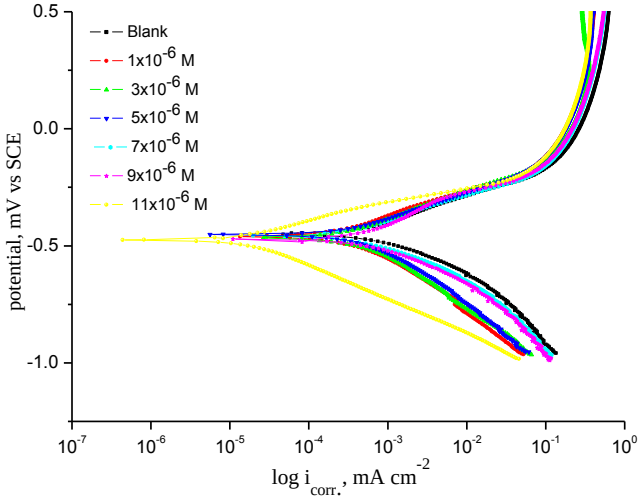

Fig. 13. Tafel polarization curves for the corrosion of steel-reinforced concretein 2 M HCl in the absence and presence of various concentrations of studied compound (H_2L) at 25 ± 0.1 °C.

Table 10. Kinetic parameters of steel-reinforced concrete in 2 M HCl at 25 ± 0.1 °C, in the presence and absence of various concentrations of H_2L.

Conc. (M)	- E_{corr} (mV vs. SCE)	$i_{corr} \times 10^{-4}$ (µA cm^{-2})	$\beta_a \times 10^{-3}$ (mV dec^{-1})	$\beta_c \times 10^{-3}$ (mV dec^{-1})	θ	% IE
Blank	449	9.27	247.0	166.3	----	-----
$1x10^{-6}$	459	3.25	166.6	175.8	0.649	64.9
$3x10^{-6}$	464	3.14	135.0	130.4	0.661	66.1
$5 x10^{-6}$	452	2.45	96.3	109.4	0.735	73.5
$7x10^{-6}$	456	0.946	46.2	41.0	0.897	89.7
$9x10^{-6}$	473	0.897	52.9	44.5	0.903	90.3
$11x10^{-6}$	474	0.861	36.1	108.4	0.907	90.7

Table 11. Parameters form electrochemical kinetic obtained by EFM method for steel-reinforced concrete in 2 M HCl with and without various concentrations of H_2L at 25 ± 0.1 °C.

Conc., M.	i_{corr} (µA cm^{-2})	$\beta_a \times 10^{-3}$ (mV dec^{-1})	$\beta_c \times 10^{-3}$ (mV dec^{-1})	CF-2	CF-3	θ	%IE
Blank	141.5	68.40	219.0	1.93	2.81	-----	------
$1x10^{-6}$	16.11	172.2	272.6	2.05	3.02	0.886	88.6
$3x10^{-6}$	15.78	116.5	236.6	1.92	3.21	0.888	88.8
$5 x10^{-6}$	14.53	90.94	134.3	2.03	2.98	0.897	89.7
$7x10^{-6}$	13.62	85.48	131.8	1.82	2.54	0.903	90.3
$9x10^{-6}$	13.50	90.68	149.1	1.69	2.95	0.904	90.4
$11x10^{-6}$	12.62	99.56	150.5	1.97	2.83	0.910	91.0

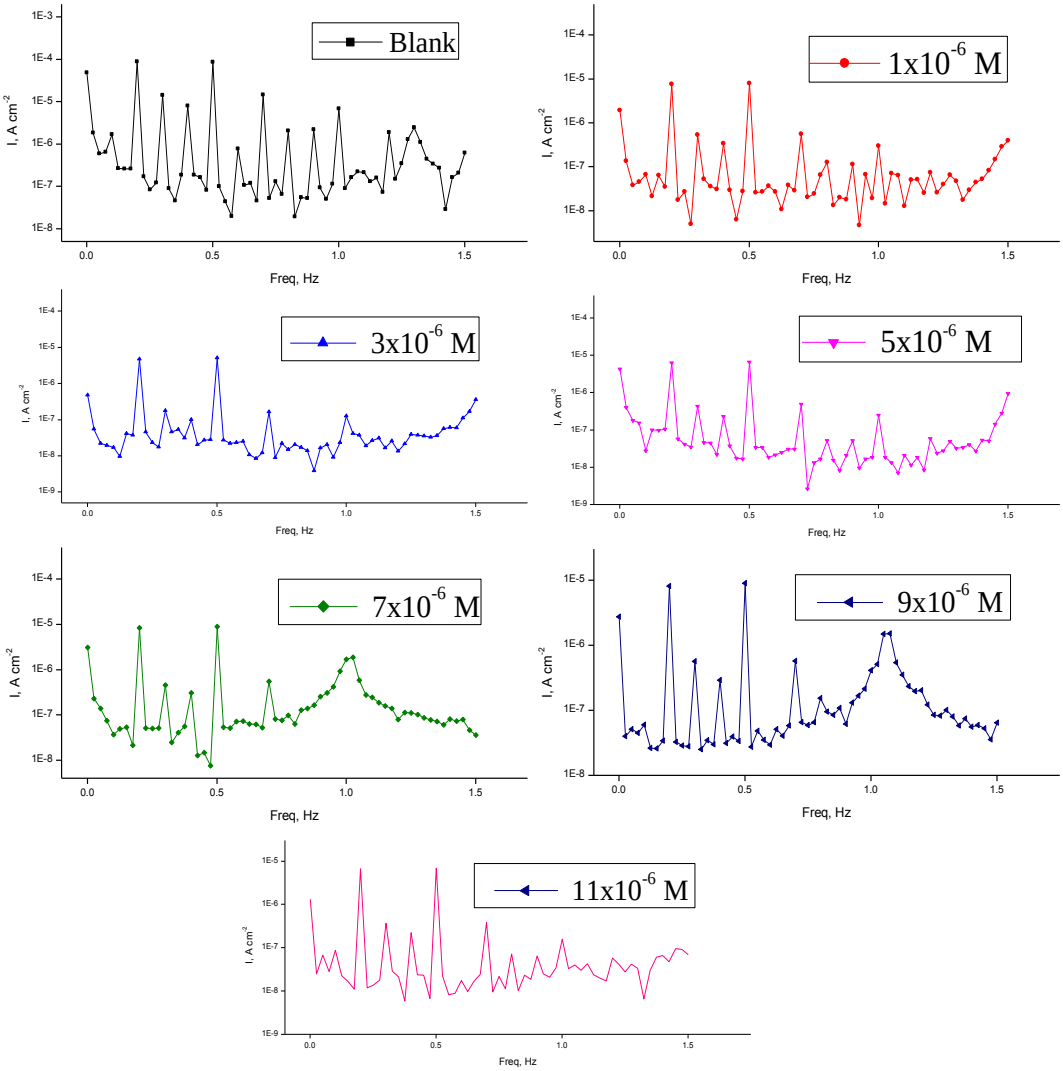

Fig. 14. EFM spectra for steel-reinforced concrete in 2 M HCl in the absence and presence of various concentrations of studied compound (H_2L) at 25 ± 0.1 °C.

Table 12. EIS data given from EIS technique for steel-reinforced concrete in 2 M HCl with and without various concentrations of H_2L at 25 ± 0.1 °C.

Conc., M.	R_S (Ω cm^2)	$Y_o \times 10^{-6}$ ($\mu\Omega^{-1}s^n$)	$n \times 10^{-3}$	R_{ct} (Ω cm^2)	$C_{dl} \times 10^{-4}$ (μFcm^{-2})	θ	%IE
Blank	1.19	62.14	854.1	980	9.07	-----	------
1x10^{-6}	9.44	123.40	794.0	1825	1.76	0.463	46.3
3x10^{-6}	11.01	123.50	741.3	1862	1.73	0.473	47.3
5 x10^{-6}	9.50	148.60	807.7	1892	1.52	0.482	48.2
7x10^{-6}	1.47	32.22	845.8	2070	1.37	0.526	52.6
9x10^{-6}	1.67	33.03	832.7	2258	1.02	0.565	56.5
11x10^{-6}	1.62	30.55	826.8	2803	1.01	0.650	65.0

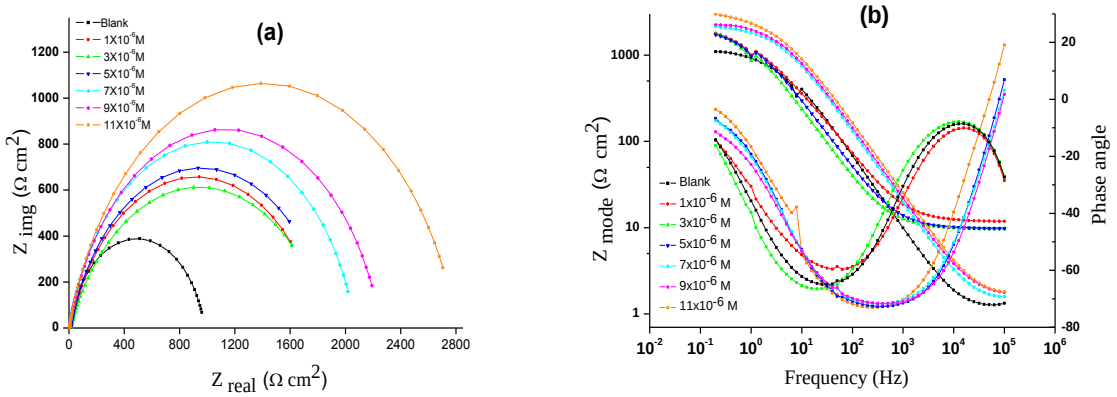

Fig. 15. EIS diagrams Nyquist plots (a) and Bode plots (b) for steel-reinforced concrete in 2 M HCl in the absence and presence of various concentrations of studied compound (H_2L)at 25 ± 0.1 °C.

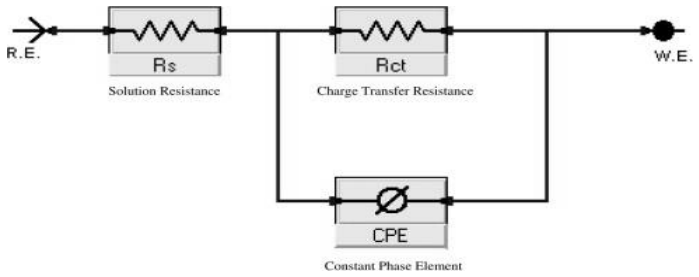

Fig. 16. Equivalent circuit model utilized to fit data spectra.

4. Conclusion

1- The synthesis of Schiff base 1-((2-hydroxyphenyl)iminomethyl)naphthalene-2-ol (H_2L) and its Cu(II), Co(II), Ni(II), Mn(II),Cd(II) and UO_2(II) complexes and characterized them by various physicochemical techniques and studied their antimicrobial activities.

2- The XRD patterns of the ligand (H_2L) and its complexes **(1, 3** and **4)** show many diffraction peaks which indicate the polycrystalline phase.

3- The thermal activation energy of decomposition (E_a) values ofthe ligand (H_2L) and its complexes was calculated.

4- The ligand showed lowest antimicrobial activity (5 mm – 7 mm) at 150 µg/mL concentration against all tested bacteria comparing to the activity of other synthetic compounds except complex **(6)** against *Klebsiella pneumoniae* and *Escherichia coli* and ligand against *Escherichia coli*, complex **(3)** against *Pseudomonas aeruginosa* and ligand and its complexes **(1, 2** and **4)** against *Klebsiella pneumoniae* which has not any antibacterial effect.

5- The ligand showed best interaction with *Staphylococcus aureus* (3q8u) receptor than the *Escherichia coli* (3t88) receptor.

6- Double layer capacitances decrease with respect to blank solution when the compound (H_2L) added. This fact may explained by adsorption of the compound (H_2L) molecule on the steel-reinforced concrete surface.

7- EFM can be utilized as a fast and nondestructive tests for calculation of corrosion without prior information of Tafel lines

8- The % E obtained from polarization curves, electrochemical impedance spectroscopy and electrochemical frequency modulation are in a good agreement.

Appendix A: Supplementary material
See the attached file.

References

1. K.K. Koo, Y.J. Jang, U. Lee, *Bull. Kor. Chem. Soc.*, **2003**, *24*, 1014.
2. R.D. Jones, D.A. Summerville, F. Basolo, *Chem. Rev.*, **1979**, *79*, 139.
3. T.D. Thangadurai, S.K. Ihm, *J. Ind. Eng. Chem.*, **2003**, *9*, 563.

4. H. Dugas, C. Penny, "Bioorganic Chemistry", Springer, New York, **1981**, p. 435.
5. M.A. Khalifa, A.M. Hassaan, *J. Chem. Soc. Pak*., **1996**, *18*, 115.
6. H.N. Aliyu, S. Sani, A.Galadima, *Appl. Chem.*, **2013**, *58*, 14696.
7. H. Naeimi, Z.S. Nazifi, *Chemija.*, **2013**, *24*, 197.
8. K. Siddappa, S.B. Mane, *J. Pharma. Pharmaceut.Sci*., **2013**, *5*, 725.
9. J.D. Margerum, L.J. Miller, "Photochromism', Wiley Interscience: New York, **1971**, p. 569.
10. E. Yousif, E. Rentschler, N. Salih, J. Salimon, A. Hameed, M. Katan, *J. Saudi Chem. Soc*., **2014** , *18*, 269.
11. B.N. Biggis, J. Lewis, "Modern Coordination Chemistry", Edited by J. Lewis & R.G. Wilkins (Interscience, New York, **1960**, 403.
12. A.Z. El-Sonbati, M.A. Diab, A.A.M. Belal, Sh.M. Morgan, *Spectrochim. Acta A*, **2012**, *99*, 353.
13. R. Shirley, "The CRYSFIRE System for Automatic Powder Indexing":User's Manual, the Lattice Press, Guildford, Surrey GU2 7NL, England, **2000**.
14. M.A. Diab, G.G. Mohamed, W.H. Mahmoud, A.Z. El-Sonbati, Sh.M. Morgan, S.Y. Abbas, *Appl. Organometal. Chem*., **2019**, *33*, e4945.
15. Sh. M. Morgan, M. A. Diab, A. Z. El-Sonbati, *Appl. Organometal. Chem*., **2018**, *32*, e4504.
16. G.G. Mohamed, A.A. El-Sherif, M.A. Saad, S.E.A. El-Sawy, Sh.M. Morgan, *J. Mol. Liq.*, **2016**, *223*, 1311.
17. H.M. Refaat, H.A. El-Badway, Sh.M. Morgan, *J. Mol. Liq*., **2016**, *220*, 802.
18. M.I. Abou-Dobara, A.Z. El-Sonbati, Sh.M. Morgan, *World J. Microbiol. Biotechnol*., **2013**, *29*, 119.
19. M.I. Abou-Dobara, N.F. Omar, M.A. Diab, A. Z. El-Sonbati, M. S. Morgan, M. A. El-Mogazy, *J. Cell. Biochem.*, **2019**, *120*, 1667.
20. A.Z. El-Sonbati, M.A. Diab, Sh.M. Morgan, M.I. Abou-Dobara, A.A. El-Ghettany, *J. Mol. Str*., **2020**, *1200*, 127065.
21. M.I. Abou-Dobara, N.F. Omar, M.A. Diab, A.Z. El-Sonbati, Sh.M. Morgan, O.L. Salem, A.M. Eldesoky, *Mat. Sc. Eng. C*, **2019**, *103*, 109727.
22. A.Z. El-Sonbati, M.A. Diab, Sh.M. Morgan, *J. Mol. Liq.* **2017**, *225*, 195.
23. S. Burt, *Inter. J. Food Microbiol*., **2004**, *94*, 223.
24. D. Close, T. Xu, A. Smartt, A. Rogers, R. Crossley, S. Price, S. Ripp, G. Sayler, *Bioreport. Sens*., **2012**, *12*, 732.
25. C.F. Carson, J. Riley, *J. App. Microbiol*., **1995**, *78*, 264.
26. H. Mith, R. Duré, V. Delcenserie, A. Zhiri, G. Daube, A.Clinquart, *Food Sci. Nutr.*, **2014**, *2*, 403.
27. B. A. Abd-El-Nabey, S. El-Housseiny, G. A. El-Naggar, E. A. Matter, G. Esmail, *J. Phy. Chem.*, **2016,** *6*, 5.
28. J. O'M. Bockris and B. Yang, *J. Electrochem. Soc.*, **1991**, *138*, 2237.
29. A.T.T. Hsieh, R.M. Sheahan, B.O. West, *Aust. J. Chem*., **1979**, *28*, 885.
30. Sh.M. Morgan, A.Z. El-Sonbati, H.R. Eissa, *J. Mol. Liq.*, **2017**, *240*, 752.
31. Sh.M. Morgan, A.Z. El-Sonbati, M.A. El-Mogazy, *Appl.Organometal. Chem*., **2018**, *32*, e4264.
32. Sh.M. Morgan, M.A. Diab, A.Z. El-Sonbati, *Appl. Organometal. Chem*., **2018**, *32*, e4305.
33. Sh.M. Morgan, M.A. Diab, A.Z. El-Sonbati, *Appl. Organometal.Chem.*, **2018**, *32*, e4281.
34. A.Z. El-Sonbati, M.A. Diab, Sh.M. Morgan, A.M. Eldesoky, M.Z. Balboula, *Appl. Organometal. Chem.*, **2018**, *32*, e4207.
35. B.H. Amin, M.I. Abou-Dobara, M.A. Diab, E.A. Gomaa, M.A. El-Mogazy, A.Z. El-Sonbati, M.S. EL-Ghareib, M.A. Hussien, H. M. Salama, *Appl. Organomet. Chem*., **2020**, *34*, e5689.
36. M.A. Diab, S.G. Nozha, A.Z. El-Sonbati, M.A. El-Mogazy, Sh.M. Morgan, *Appl. Organomet. Chem*., **2019**, *33*, e5153.
37. A.Z. El-Sonbati, M.A. Diab, Sh.M. Morgan, H.A. Seyam, *J. Mol. Str*., **2018**, 1154 , 354.
38. A.B.P. Lever, "Inorganic Electronic Spectroscopy", Second Ed., Elsevier Publishing, New York, **1984**.
39. A.Z. El-Sonbati, W.H. Mahmoud, G.G. Mohamed, M.A. Diab, Sh.M. Morgan, S.Y. Abbas, *Appl. Organometal. Chem*., **2019**, *33*, e5048.

40. A.Z. El-Sonbati, M.A. Diab, A.A. El-Bindary, G.G. Mohamed, Sh.M. Morgan, M.I. Abou-Dobara, S.G. Nozha, *J. Mol. Liq*., **2016**, *215*, 423.
41. S.P. McGlynn, J.K. Smith, W.C. Neely, *J. Chem. Phys*., **1961**, *35*, 105.
42. R.M. Silverstein, G.C. Bassler, T.C. Morrill, "Spectrophotometric Identification of Organic Compounds", 4th Edn., Wiley, New York, **1981**.
43. A.B.P. Lever, D. Ogden, *J. Chem. Soc*., **1967**, 2041.
44. N.A. El-Ghamaz, M.A. Diab, A.Z. El-Sonbati, Sh.M. Morgan, O.L. Salem, *Chem. Pap*., **2017**, *71*, 2417.
45. A.Z. El-Sonbati, M.A. Diab, A.M. Eldesoky, Sh.M. Morgan, O.L. Salem, *Appl. Organometal. Chem*., **2019**, *33*, e4839.
46. A.Z. El-Sonbati, M.A. Diab, G.G. Mohamed, M.A. Saad, Sh.M. Morgan, S.E.A. El-Sawy, *Appl. Organometal. Chem.*, **2019**, *33***,** e4973.
47. Sh.M. Morgan, N.A. El-Ghamaz, M.A. Diab, *J. Mol. Struct*., **2018**, *1160*, 227.
48. A.B.P. Lever, "Inorganic Electronic Spectroscopy", (Elsevier, Amestrdam) **1968**.
49. M.A. Diab, A.Z. El-Sonbati, Sh.M. Morgan, M.A. El-Mogazy, *Appl. Organometal. Chem*., **2018**, *32*, e4378.
50. B.N. Figgs, "Introduction to Ligand Field", Wiley Eastern Ltd, India, **1976**, p. 163.
51. A.Z. El-Sonbati, M.A. Diab, Sh.M. Morgan, M.A. El-Mogazy, Appl. Organometal. Chem., **2018**, *32*, e4530.
52. A.Z. El-Sonbati, M.A. Diab, Sh.M. Morgan, M.Z. Balboula, *Appl. Organometal.Chem.*, **2018**, *32*, e4059.
53. T. Chattopadhyay, M. Mukherjee, K.S. Banu, A. Banerjee, E. Suresh, E. Zangrando, D. Das, Journal of coordination chemistry **2009**, *62*, 967.
54. P. Swati, R. Singh, I.K. Karnawat, Sharma, P.S. Verma, *J. Chem. Tech.Res*., **2011**, *3*, 1164.
55. N.A. El-Ghamaz, A.Z. El-Sonbati, Sh.M. Morgan, *J. Mol. Struct*., **2012**, *1027*, 92.
56. A.Z. El-Sonbati, A.A.M. Belal, M.S. El-Gharib, Sh.M. Morgan, *Spectrochim. Acta A*, **2012**, *95*, 627.
57. R. John Dyer, "Application of Absorption Spectroscopy of Organic Compounds", Prentic Hall.New Delhi, **1984**.
58. S. Basak, A. Mondal, D. Chopra, K.K. Rajak, *Polyhedron*, **2007**, *26*, 3465.
59. M.I. Issa, M.R. Issa, M.Y. Temark, M.M. Ghonium, *Egypt. J. Chem*., **1975**, *18*, 11.
60. G. Karagonius, O. Pete, Z. Electrochem, B.Bunsenges, *Phys. Chem*., **1959**, *63*, 1170.
61. A.Z. El-Sonbati, *Synth. React. Inorg.Met.-Org. Chem*., **1991**, *21*, 977.
62. A.W. Coats, J.P. Redfern, *Nature*, **1964**, *201*, 68.
63. H.H. Horowitz, G. Metzger, *Anal. Chem*., **1963**, *35*, 1464.
64. M.A. Diab, A.Z. El-Sonbati, N.A. El-Ghamaz, Sh.M. Morgan, O. El-Shahat, *Eur. Polym. J*., **2019**, *115*, 268.
65. World Health Organization (WHO). Fact sheet No: 125, http: //www.who.int/mediacentre/ factsheets/fs125/en/index.html.Enterohaemorr h agic Escherichia coli (EHEC). World Health Organisation, Geneva, **2011**.
66. R. Seenivasan, H. Indu, G. Archana, S.Geetha, *J. Agric. Environ. Sci*., **2010**, *9*, 480.
67. H. Nikaido,*Mol. Biol*., **2013**, *67*, 593.
68. H. Nikaido, *Science*, **1994**, *264*, 382.
69. D.J. Stickler, *Soc Appl Microbiol.*, **2002**, *31*, 163.
70. I.H. Kim, D.G. Lee, S.H. Lee, *Biotechnol. Biopro.Eng*., **2007**, 12, 579.
71. T.A. Ayandrian, A.A. Ayandele, S.O. Dahunsi, O.O. Ajala, *J. Aquatic Res*., **2014**, *40*, 291.
72. R.S. Graham, K.F.Bott, *Mol. Gen.Genet*., **1975**, *137*, 227.
73. S. Miller, *molecules. Bio*., **2016**, *7*, e0154116.
74. A. Yoshimi, K. Miyazawa, K. Abe, *Biotechnol.Biochem. J*., **2016**, *80*, 1700.
75. A.S. El -Fatimi, H.A. El -Gahmi, M.M. Godeh, A.M. Bleibi, S. Abd El –Moneim, *J. Exp. Biol. Bot*., **2013**, *9*, 75.
76. S. Li, R.R. Breaker, *Bioorg .Med. Chem. Lett*., **2012**, *33*, 3317.
77. S.H. Lim, I. Darah, K. Jain, S. Suraya,*J. Appl. Pharm. Sci.*, **2011**, *1*, 75.
78. I. Darah, M. Nisha, S.H. Lim, *Appl. Biochem. Biotechnol*., **2015**, *175*, 2629.
79. S.G. Nozha, Sh.M. Morgan, S.E. Abu Ahmed, M.A. El-Mogazy, M.A. Diab, A.Z. El-Sonbati, M.I. Abou-Dobara, *J. Mol. Struct.*, **2021**, *1227*, 129525.
80. A.Z. El-Sonbati, M.A. Diab, S.Y. Abbas, Gehad G. Mohamed, Sh.M. Morgan, *Egypt. J. Chem.*, **2021,** *64*, 4125.

81. S. A. Pauline, S. Sahila, S. Nanjundan, N. Rajendran., *J. Progress in Organic Coatings.*, **2011**, *72*, 443.
82. M. Antonijevic, M. Radovanovic, *J. Electrochem. Soc.*, **2009**, *4*, 654.
83. A.M. Eldesoky, M.A. Diab, A.Z. El-Sonbati, S.F. Salam, *Int. J. Electrochem. Sci.*, **2017**, *12*, 4215.
84. A. S. Fouda, M. A. Diab, A.Z. El-Sonbati, Sh. A. Hassan, *Int. J. Electrochem. Sci.*, **2017**, *12*, 5072.
85. D.C. Silverman, J.E. Carrico, *J. Corrosion*, **1988**, *44*, 280.
86. D.D. Macdonald, M.C.H. Mckubre, "Impedance measurements in electrochemical systems "Modern Aspects of Electrochemistry, (J.O'M. Bockris, B.E. Conway, R.E. White, Eds., PlenumPress, New York, **1982**, 61.
87. M. Mahdavian, M.M. Attar, *J. Corros. Sci.*, **2006**, *48*, 4152.
88. G. Barral, S. Maximovitch, C. Montella, *J. Applied Electrochemistry*, **1991**, *21*, 991.
89. Q. Zhang, Y.X. Hua.,. *J. Electrochimica Acta.*, **2009**, *54*, 1881.
90. R. Solmaz, *J. Corros. Sci.*, **2014**, *79*, 169.
91. H.A. Sorkhabi, N.G. Jeddi, F. Hashemzadeh, H. Jahani., *J. Electrochimica Acta.*, **2006**, *51*, 3848.
92. E. Kus and F. Mansfeld, *J. Corros. Sci.*, **2006**, *48*, 965.
93. G.A. Caigman, E.M. Holt, *J. Chem. Cryst.*, **2002**, *32*, 315.
94. A.M. Eldesoky, M.A. El-Bindary, A.Z. El-Sonbati, Sh.M. Morgan, *Journal of Materials and Environmental Science*, **2015**, *6*, 2260.
95. M.A. Hegazy, M. Abdallah, H. Ahmed, *J. Corros. Sci.*, **2010**, 52, 2897.
96. A.S. Fouda, G Y El-Ewady, A.S. Abousalem, *J. Der Pharma Chemica.*, **2015**, *7*, 183.
97. C. Lee, W. Yang, R. G. Parr, *J. Phys. Rev. B.*, **1988**, *37*, 785.
98. Ahmed A. El-Sonbaty, Ahmed A. Al-Sarawy, Mostafa A. Diab, Mahmoud H. Mahmoud, *Egypt. J. Chem.*, **2021**, *64*, 807.
99. D.K. Yaday, B. Maiti, M.A. Quraishi, *J. Corros. Sci.*, **2010**, *52*, 3586.